3D array processing for infrasound arrays with non-ground based detectors

Rens Marcus Maria Reus

for the degree of Master of Science
in Applied Geophysics at
Delft University of Technology
ETH Zürich
RWTH Aachen University

Delft University of Technology
Faculty of Civil Engineering and Geosciences
14th May 2020

IDEA LEAGUE
JOINT MASTER'S IN APPLIED GEOPHYSICS

Delft University of Technology, The Netherlands
ETH Zürich, Switzerland
RWTH Aachen, Germany

Dated: 14th May 2020

Supervisors:

Prof. Dr. L.G. Evers
Ir. P.S.M. Smets

Committee Members:

Prof. Dr. L.G. Evers
Dr. Ir. P.S.M. Smets
Dr. C. Schmelzbach

Abstract

Array processing of infrasound data uses the coherency between sensors to calculate directions of incoming waves. The Cabauw Infrasound Array (CIA) provides unique opportunities for infrasound processing. Because unlike most infrasound arrays, CIA has sensors with height differences. Specifically sensors distributed on a 200m tall tower. But the data from these tower sensors are of limited use for time-domain array processing due to the measurement of both the incoming wave and its reflection. To make the measurements suitable for array processing the reflection needs to be removed. The ground measurements are used to approximate the waveform and a time-shifted ground average is removed from the tower measurements. The new cleaned data was successfully used for full 3D array processing.

Contents

1 Introduction

1.1 Infrasound

Infrasound is acoustic waves below 20Hz and above 0.01Hz. Above 20Hz humans can hear it and it is considered sound. Below 0.01Hz gravity begins to affect the sound waves and from 0.002Hz gravity becomes dominant[Gossard and Hooke, 1975], waves in these ranges are called acoustic-gravity and gravity waves respectively. Low-frequency waves has lower attenuation and propagates far. An extreme example is the explosion of Krakatoa in 1883. The pressure wave from this explosion propagated around the world 3.5 times[Symons et al., 1888]. The long-distance propagation made infrasound a suitable verification technique for the Comprehensive Nuclear-Test-Ban Treaty (CTBT). The CTBT was signed in 1996. Monitoring is done by four different methods, Seismological, hydro-acoustical, radionuclide and infrasound measurements[Christie and Campus, 2010]. The International Monitoring System (IMS) was established to monitor for signals from nuclear explosions. The infrasound part of the IMS will consist of a 60-station infrasound monitoring network uniformly distributed over the globe. The IMS not only measures infrasound from nuclear explosions but also many other sources like volcanoes, rocket launches [Edwards and Green, 2012], chemical explosions, (jet) aeroplanes [Smink et al., 2019], hydro-power plants and industry [Liszka, 1974]. The measurements can be used for atmospheric investigations, determining the location and energy of volcanic eruptions and severe storms[Bedard and Georges, 2000]. The construction of the IMS has lead to a renewed interest in infrasound research.

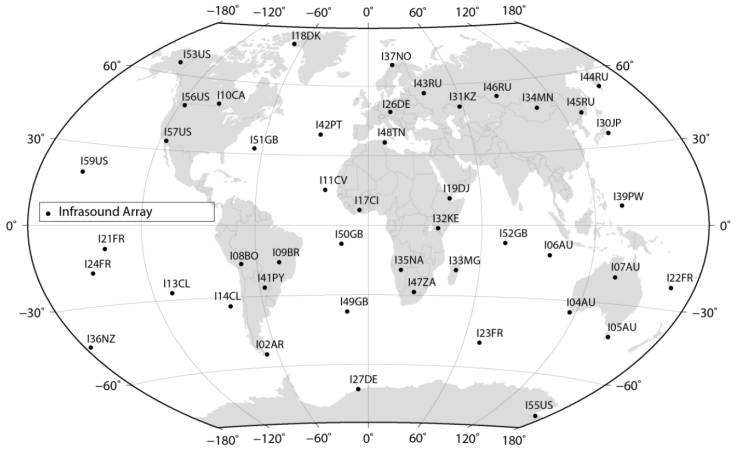

Figure 1: IMS infrasound arrays as of August 2014[Gibbons et al., 2015]

1.2 Array Processing

Infrasound stations are arrays, made up of multiple detectors. The detectors are pressure sensors, examples of sensor distribution for multiple IMS arrays in Figure 2. The coherency between measurements can evaluated using the Fisher ratio [Melton and Bailey, 1957]. The direction and speed of a signal can be reconstructed using delay and sum beamforming or array processing. Different delays are applied to the measurements. The delays are calculated using the relative positions of the detectors and a slowness vector that describes the direction and speed of an infrasound wave. This calculation will be done for a set of slowness vectors. The coherency calculations will be applied to multiple overlapping time windows to see its evolution over time. If a strong signal is present, array processing will return a coherent slowness vector.

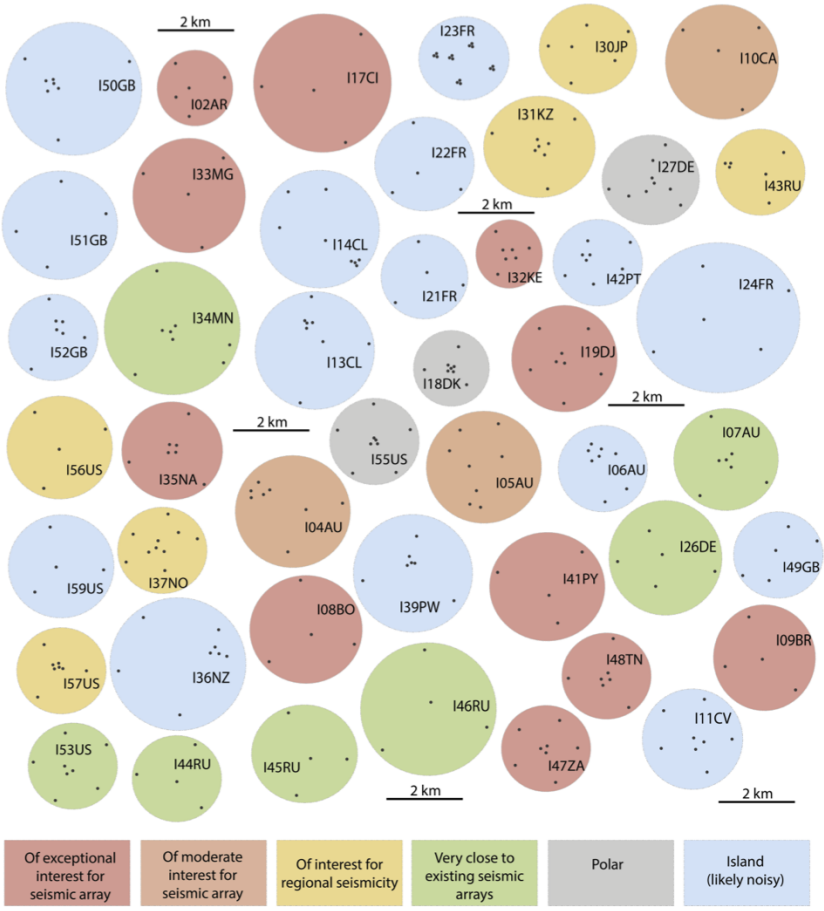

Figure 2: Several infrasound array shapes and sizes [Gibbons et al., 2015]

If a signal is strong enough to detect by multiple stations the location of the

source can be recovered using triangulation.

Array processing can be done with 2D and 3D slowness vectors. Most infrasound stations have little to no elevation difference between the sensors[Edwards and Green, 2012]. This allows the search to be limited to 2D slowness vectors and reduces computation time. The back azimuth and the apparent velocity can be calculated from the slowness vector. The apparent velocity can be significantly higher than the speed of sound due to the angle of the wave with the XY-plane. When elevations differences become large enough ignoring the vertical component can introduce errors. This is the case for some IMS stations where the local topology doesn't allow for a flat array[ibid.]. Chapter 2.4 will show an example of this and a more detailed explanation of the workflow.

1.3 Non surface-based sensors

The Cabauw Experimental Site for Atmospheric Research (CESAR) is a meteorological research centre operated by the Royal Netherlands Meteorological Institute (KNMI). A 213 m high mast is the central feature of this site. The tower was specifically built at the Cabauw site for meteorological research to establish relations between the state of the atmospheric boundary layer (ABL), land surface conditions and the general weather situation for all seasons[*About Cesar Observatory* n.d.]. A more recent addition is the Cabauw Infrasound Array (CIA). It consists of 10 ground sensors and 5 sensors on the tower. This geometry provides unique opportunities and problems. The vertical resolution of the array makes it possible to measure the vertical component of the slowness vector. But because the sensors on the tower are not ground-based the wave passes the sensors twice. The second time due to the reflection from the ground. This causes interference in the measurements. Array processing won't work properly anymore when the measurements from the tower are included. This objectives of this thesis are to remove the reflected signal from the tower measurements, use the cleaned measurements in the beamforming process and asses its usability and limitations.

1.4 Thesis outline

After the introduction, the thesis contains the following chapters. Chapter 2 describes the theory of array processing. The geometries involved with 2D and 3D processing. A derivation of the Fisher ratio. And finally an example of array processing where the effects of height differences introduce an error in 2D processing. Chapter 3 explains the unique properties of the Cabauw Infrasound array, presents a method to remove reflections from the data. In chapter 4, the results from array processing with the cleaned measurements are presented. Finally, chapter 5 provides an analysis of the array processing results. It discusses the limitations of the reflection removal, suggestions for improvements and further research.

2 Theory

2.1 Array Processing

When processing the data the assumption is made that the source of the infrasound is far away compared to the aperture of the array. This means that the incoming infrasound wave can be treated as a 3D plane wave. The planar wave will move across the array and will be detected at different times by different sensors depending on the slowness of the wave and the coordinates of the sensor, Figure 3[Smets, 2018].

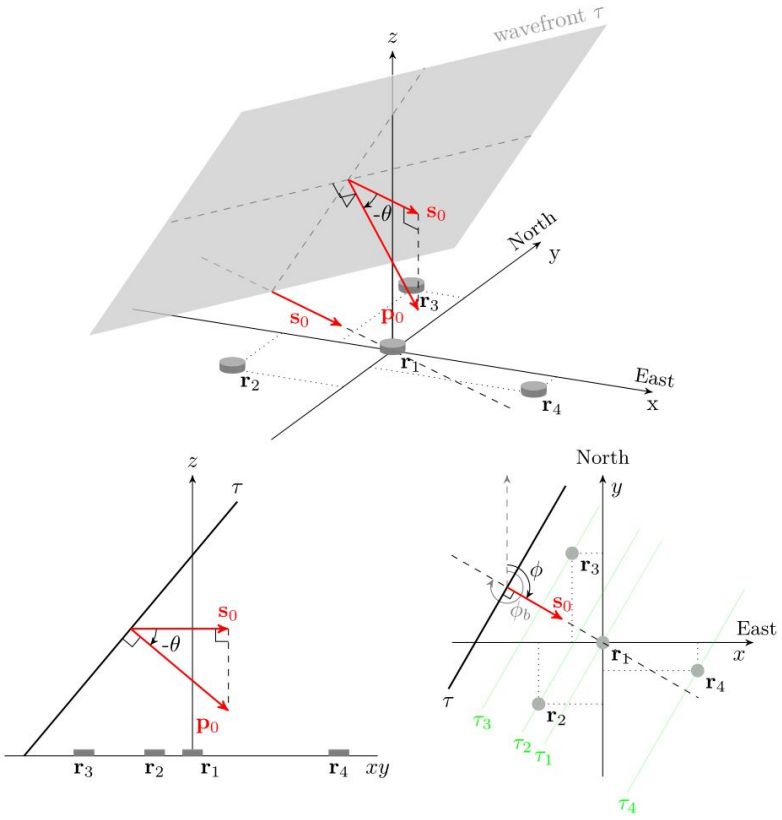

Figure 3: A plane wave propagating along an array.[Smets, 2018]

The slowness vector is defined as,

$$\vec{p} = \begin{pmatrix} p_x \\ p_y \\ p_z \end{pmatrix} = \frac{1}{c_{eff}} \begin{pmatrix} \cos(\theta)\sin(\phi) \\ \cos(\theta)\cos(\phi) \\ \sin(\theta) \end{pmatrix}, \tag{1}$$

where ϕ is the azimuth, the angle with respect to the north, θ is the inclination,

the angle with respect to the horizontal plane and c_{eff} the effective speed of sound.

$$c_T = \sqrt{\gamma R T}, \tag{2}$$

with γ, the heat capacity ratio, R the gas constant, and T the temperature of dry air. γ is 1.4 and R is 286.85 J/kgK and when filled in equation 2 simplifies to,

$$c_T = 20.04\sqrt{T}. \tag{3}$$

To get the effective speed of sound, that is the actual velocity that the infrasound waves have with respect to the array the windspeed needs to be added.

$$c_{eff} = c_T + \vec{u_{xy}} \cdot \hat{n}_{xy} \tag{4}$$

with $\vec{u_{xy}}$ the horizontal wind velocity and $\hat{n}_{xy}$ the direction of the infrasound wave.

The projection of p onto the XY-plane is

$$\vec{s} = \begin{pmatrix} p_x \\ p_y \end{pmatrix} = \frac{1}{c_a pp} \begin{pmatrix} \sin(\phi) \\ \cos(\phi) \end{pmatrix}, \tag{5}$$

with

$$c_{app} = \frac{c_T}{cos\theta}, \tag{6}$$

the apparent velocity in the XY-plane. c_{app} ranges from c_T at θ equals 0° up to infinity for an angle of 90° The speed of sound depends on heat capacity ratio, the gas constant and temperature of air.

The plane wave is detected at different times by the different sensors. The time difference between two sensors $\Delta t = t_1 - t_2$ depends on the slowness of the plane wave and the coordinates of the sensors,

$$\Delta t = \vec{p} \cdot (\vec{r_1} - \vec{r_2}), \tag{7}$$

where $\vec{r_1}$ and $\vec{r_2}$ are coordinates of the respective sensors. To simplify the time difference for each sensor is calculated with respect to a central point,

$$\tau_i = \vec{p} \cdot \vec{r_i}, \tag{8}$$

where τ_i and r_i are the relative time shift and coordinates for sensor i with respect to the centre of the array. The time delay can be broken up into a vertical and horizontal component.

$$\tau_i = \tau_H + \tau_z, \tag{9}$$

with

$$\tau_H = p_x r_x + p_y r_y, \tag{10}$$

and

$$\tau_V = p_z r_z, \tag{11}$$

Due to the digital nature of the measurements, the only integer multiples of one sample period shows up. This can cause limitations when trying to undo the time shifts if shifts of smaller than one sample period are needed. An example of this occurs in 2.4 where the measurements are interpolated to allow for subsample shifting.

For sets of delays the The direction and speed of a signal can be reconstructed using array processing. The measurements get shifted in time. Sets of delays get calculated based on slowness vectors. Each set gets a coherency rating, the Fisher ratio. A high Fisher ratio indicates a signal is present in the data. The slowness vector with the highest coherency value will point to the origin of the signal. Array processing is applied for different time windows. For each window coherency values are calculated. This provides the signal strength over time.

2.2 Array Response

A monochromatic wavefield of unit amplitude is described by,

$$g(t, \vec{x}) = e^{i(\omega_0 t - \vec{k_0} \cdot \vec{x})} \tag{12}$$

, with t the travel time, ω_0 the angular frequency, $\vec{k_0}$ the wave number and $\vec{x}$ the position of the wave.

The Fourier transform of equation 12 is

$$G(f, \vec{x}) = \int_{-\infty}^{\infty} g(t, \vec{x}) e^{-i\omega t} dt = \delta(f - f_0) e^{-i\vec{k_0}\vec{x}} \tag{13}$$

The wavefield can be characterized as a frequency-wavenumber (f/k) spectral density function. For a planar array this is given by([Denholm-Price and Rees, 1999]),

$$E(\vec{k_{xy}}, f) = \int_{-\infty}^{\infty} \int_{-\infty}^{\infty} G(f, \vec{r_{xy}} e^{i(k_{xy} \cdot \vec{r_{xy}})}) dx dy, \tag{14}$$

where $\vec{r_{xy}}$ are the sensor positions on the ground.

The discrete form of the frequency-wavenumber power spectrum is defined as [Smart and Flinn, 1971]:

$$E(\vec{k_{xy}}, \omega) = \left| \sum_{n=1}^{N} G(\vec{r_n}, \omega) e^{i\vec{k_{xy}} \cdot \vec{r_n}} \right|^2 \tag{15}$$

Substituting equation 13 in to 15 sampled by N senors, yields the array response,

$$R(\vec{p}, \omega) = \left| \frac{1}{N} \sum_{n=1}^{N} e^{-i\omega(\vec{p} - \vec{p_0}) \cdot \vec{r_n}} \right|^2, \tag{16}$$

with p_0 the slowness vector of the plane wave and ω the angular frequency. R is a theoretical measure for the best estimate or sensitivity of receivers $\vec{r_n}$ to plane wave $\vec{p_0}$ represented by an infinite aperture array regularly sampled in $\vec{p}$. The

array response depends on the number of and locations of sensors. An array design can affect its sensitivity to different slowness vectors. Figure 4 show 3 array shapes and their array responses. Each of the figure show the response for a wave coming from directly above, $s = (0, 0)$. The first shows a smaller array with a higher accuracy in one direction. The axis with the smaller aperture show a bigger spread in p values with high coherency values. The second shows a larger symmetrical array. The main lobe is smaller but due to its size some secondary lobes show up that also provide high coherency values. Secondary lobe can be suppressed by adding extra sensors as seen in the third figure.

2.3 Fisher Ratio

The Fisher ratio describes the coherency a group of measurements. It was first described in [Melton and Bailey, 1957]. It was based on work done by [Fisher, 1948] and named in honour of him. Given N time-shifted recordings each with a T number of samples each denoted by x_{nt}. The average as a function of time is defined as,

$$x_t = \frac{1}{N} \sum_{n=1}^{N} x_{nt}, \tag{17}$$

and the total average is,

$$x = \frac{1}{NT} \sum_{t=1}^{T} \sum_{n=1}^{N} x_{nt}. \tag{18}$$

This is also the constant offset or bias of all the measurements. Fisher statistics make use of the variances of the recordings. The total variance is

$$V_T = \frac{1}{NT} \sum_{t=1}^{T} \sum_{n=1}^{N} (x_{nt} - x)^2 \tag{19}$$

which can be split up into two parts

$$V_T = V_W + V_B, \tag{20}$$

where

$$V_W = \frac{1}{NT} \sum_{t=1}^{T} \sum_{n=1}^{N} (x_{nt} - x_t)^2, \tag{21}$$

is the variation within a recording and

$$V_B = N \sum_{t=1}^{T} (x_t - x)^2, \tag{22}$$

is the variation between recordings. V_W is a measure for the amount of noise as it compares the total average with each measurement. V_B compares the total

average with the average across time which results in a measure of the signal strength. Combining these two equations gives the formula for the Fisher ratio,

$$F = \frac{T(N-1)}{T-1}\frac{V_B}{V_W}. \tag{23}$$

The signal-to-noise ratio can be derived from the Fisher ratio,

$$SNR = \sqrt{\frac{F-1}{N}} \tag{24}$$

2.4 Array processing Example

I18DK is an example of an infrasound array where elevation difference are big enough to introduce an error in 2D array processing. It's an 8 sensor array located in Greenland. The relative coordinates of the sensors are shown in table 1. The array has an aperture of 1170m and a maximum height difference of 110m. The sample rate of the sensors is 20Hz. To demonstrate the effects of elevation differences 2 events will be processed. The launch of the Space Shuttle Discovery from the mission STS-131 on 2010/04/05 and the eruption of Kasatochi on 2008/08/07. The final results will be a reproduction of the results from [Edwards and Green, 2012].

x	y	z
-63.96	69.64	-12.56
96.11	40.61	5.44
79.16	-102.29	-19.56
-65.18	-84.43	-15.56
15.23	-7.40	21.94
205.78	564.21	74.44
418.27	-433.87	-35.56
-685.40	-46.47	-18.56

Table 1: Relative coordinates of I18DK infrasound sensor with respect to center.

2.4.1 Preprocessing

The raw data is unsuitable to be processed by the array processing algorithm. This is due in part to the presence of noise, local pressure differences and the detector response. The response characteristics of the detectors were removed. A band-pass filter between 0.06 and 1Hz is applied for STS-131 and between 0.03 and 0.3HZ for Kasatochi. The data is demeaned and the measurements are interpolated to 100Hz using Lanczos resampling to allow for subsample shifting.

2.4.2 Slowness Grid

A choice needs to be made what set of slowness vectors to try out. This can be done in a simple rectangular grid of p_x and p_y. Alternatively, the choice for a grid in polar coordinates (ϕ, c_{app}) can be made, Figure 5. Both of these are sensitive to all directions. If only a certain direction is of interest a subset of the grid can be used.

For 3D slowness vectors, a similar choice can be made between a grid in Cartesian coordinates or spherical coordinates (ϕ, θ, c_{eff}).

Because this section will show the difference between 2D and 3d processing 2 separate grids will be used and the entire workflow except the preprocessing will be done twice. To ensure unique solution a c_{eff} needs to be chosen for the 3D processing. These $320m/s$ and $330m/s$ for STS-131 and Kasatochi respectively. Since this is a replication of an earlier paper the approximate direction and velocity of the signal are known only a subset of slowness vectors are evaluated.

2.4.3 Shifting

For each sensor-slowness combination, a time shift is calculated as described in equation 8. Because the data is not continuous but discrete this limits the sample shift to integer values. This, in turn, limits the number of slowness vectors that produce unique sets of shifts. This is where the interpolation mentioned in the preprocessing comes in. Applying an interpolation to the measurements allows for subsample shifting. Even though the sample rate of the sensors is only 20Hz the delays between sensors won't be exact multiples $1/f$ and differences smaller than the sample period still affect the measurements and cause changes in the coherency value for shifts smaller than the sample period. The interpolation allows more different slowness vectors to be evaluated and provide more accurate results but it increases processing time.

2.4.4 Time windows

For each slowness, the coherency value is calculated using the shifted measurements as input. To get the coherency, as well as the back azimuth and c_{app}, as a function of time this is done for separate time windows. The window length is 60 seconds for STS-131 and 120 seconds for Kasatochi and both have an overlap of 0.9. The overlap helps to make sure a waveform doesn't get split up between windows and provides a more granular view of the data at the cost of more processing. The back azimuth and c_{app} are calculated from the slowness vector with the highest coherency within a window.

2.4.5 Results

Figure 6 shows the back azimuth, apparent velocity and the coherency value (F) over time. The grey values correspond to the results from the 2D process and the black values to the 3D process. The time shifts that return the highest coherency are almost the same for the 2D and 3D process but due to the z-component of

the slowness and the elevation of the detector these shifts correspond to different slowness vectors. This results in a positive error for the apparent velocity in the STS-131 case. The error comes from the fact that the 2D process needs to compensate for the time difference caused by the vertical components of the slowness. Depending on the geometry of the array and the direction of the wave the error can also occur in the back azimuth as is the case for the Kasatochi eruption.

Figure 7 shows the results from 2D and 3D beamforming of the Kasatochi eruption. This time the measured signal came from a different direction. Now the 2D process has the highest coherency value for a slowness that is from a slightly wrong angle. This is the 'incorrect' 2D slowness that corresponds to the same time shifts as the 'correct' 3D slowness vector.

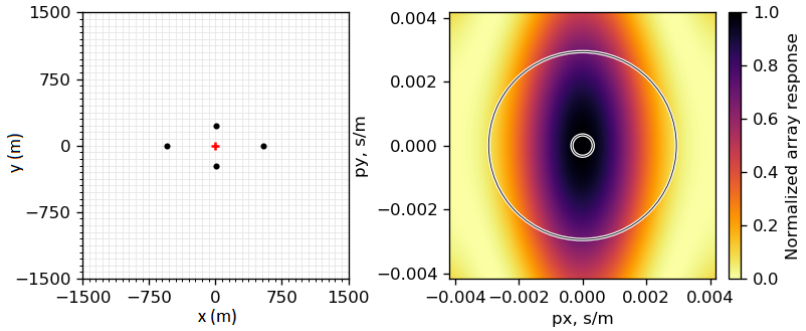

(a)

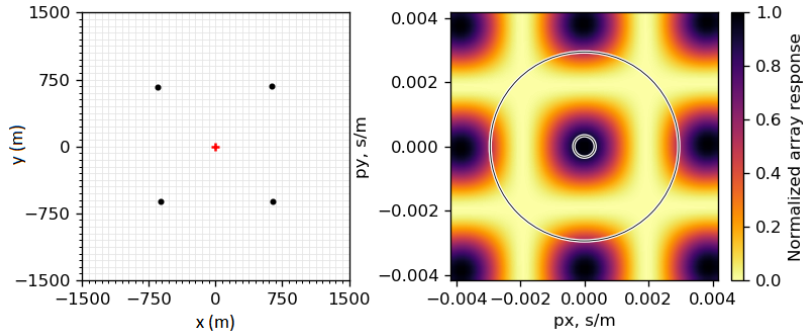

(b)

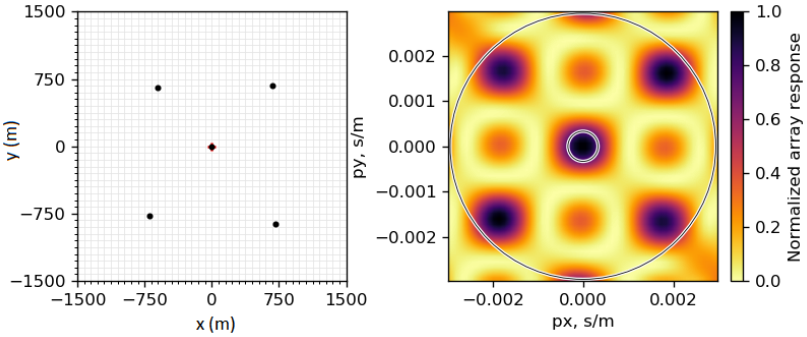

(c)

Figure 4: Array responses of several difference layouts

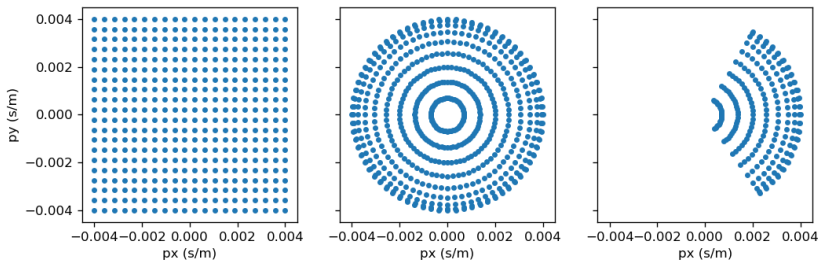

Figure 5: Examples of 2D slowness distributions

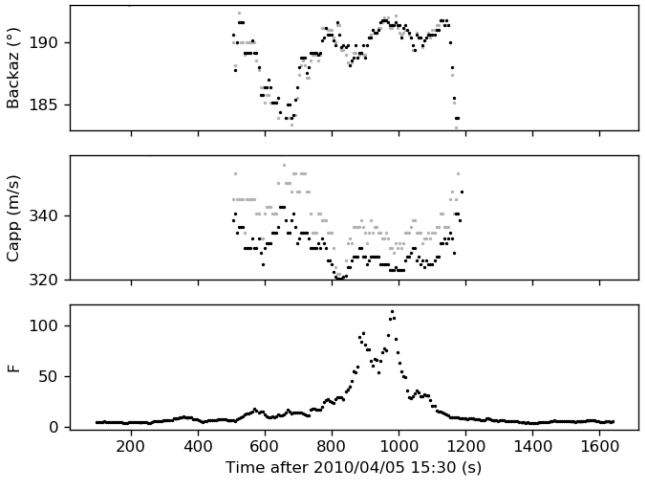

Figure 6: Comparison of results between 2D and 3D processing. STS-131

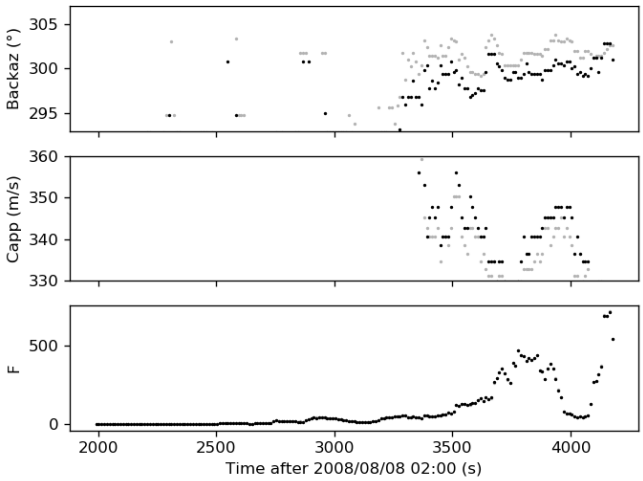

Figure 7: Comparison of results between 2D and 3D processing. Kasatochi

3 Non surface-based detectors

The Cabauw Infrasound Array (CIA) consists of 15 detectors, 10 detectors on the ground and 5 detectors distributed along a 200m tall tower. The detectors are shown in Figure 8a with the location of the tower indicated by T. The sensor that were not used or not active are greyed-out.

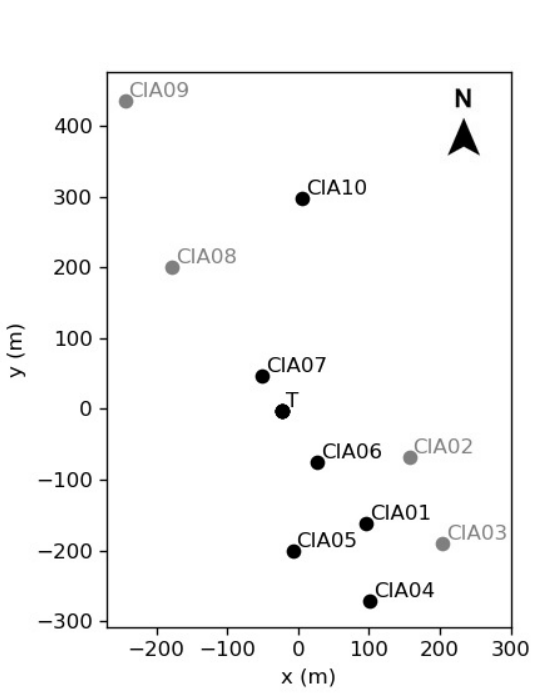

(a) Distribution of sensors at Cabauw

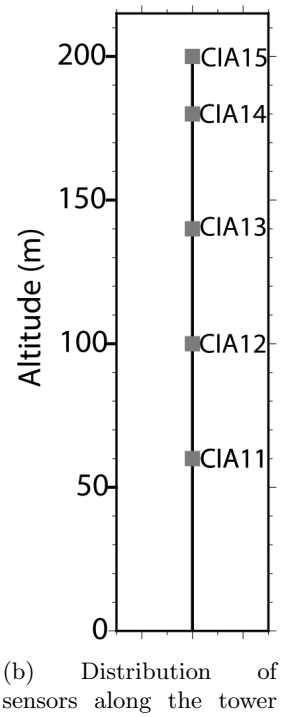

(b) Distribution of sensors along the tower [Smink et al., 2019]

Figure 8: Distribution of sensors at Cabauw

This unique setup allows for the vertical slowness, p_z, to be measured. This can be done without needing to assume the effective velocity, like in the Greenland example. In Figure 9 the preprocessed measurements from 4 sensors are shown, two ground sensors CIA01 and CIA10, which show the same waveform except for a temporal offset, and two tower sensors CIA12 and CIA14, which also some an increased amplitude around the same time but these waveforms have quite different shapes compared to each other and the ground measurements. The effect is caused by the signal passing by the tower sensors twice, the second being the reflection from the ground. The original signal and the reflection partially overlap. The amount the overlap depends on the height of the sensors. This causes interference and lowered coherency values when including the data from the tower sensors and causes the array processing to stop properly functioning. [Smink et al., 2019] showed that the measurements from

the tower sensors can be approximated by adding a time-shifted version of the ground measurement to itself. This simulates the added travel time of the reflection. This implies that a reverse of this process can be done by removing a time-shifted version, the reflection, from the tower measurements leaving tower measurements with only the incoming signal.

3.1 Removal of reflections

Figure 9 shows higher amplitudes for the ground sensor compared to the tower sensors. This difference between the tower and ground sensors can be explained by the fact that the ground stations are in a reflection point which causes a doubling of the amplitude, [Pierce, 1990, chapter 3]. When trying to remove the reflection for the tower measurements this difference needs to be compensated for otherwise, the removal will have a greater amplitude than the actual reflection in measurement. This is done by doubling the amplitudes of the tower measurements. Doubling the tower measurements also ensures they are given equal weight to the ground measurements. To approximate the true waveform of the signal a beamform of the ground measurements is made, Figure 10. This beamform is made by using the 2D slowness vector with the highest coherency value from the processing using only the ground stations.

The ground around the array is assumed to be perfectly reflective and flat. In this case, it follows from Snell's law that the angle of incidence equals the angle of reflection[ibid.]. Expressed in slowness coordinates it means that the only change in the slowness vector is a sign flip of p_z.

To remove the reflection from the measurements the ground beamform is shifted to the coordinates of the tower sensors subtracted from the tower measurements. Figures 11 and 12 show the measurements from each of the tower sensors before and after the removal of the reflection in black compared with the ground beamform, which is the same in each of the plots, in grey. It only the bump from the incoming signal remains and the reflection is no longer present with in the data.

Then the ground data and reflection filtered tower data are used for full 3D array processing to resolve the vertical component of the slowness. After this process coherency values are calculated for the ground data, the tower data and everything together. Results from the 3D array processing in the next chapter.

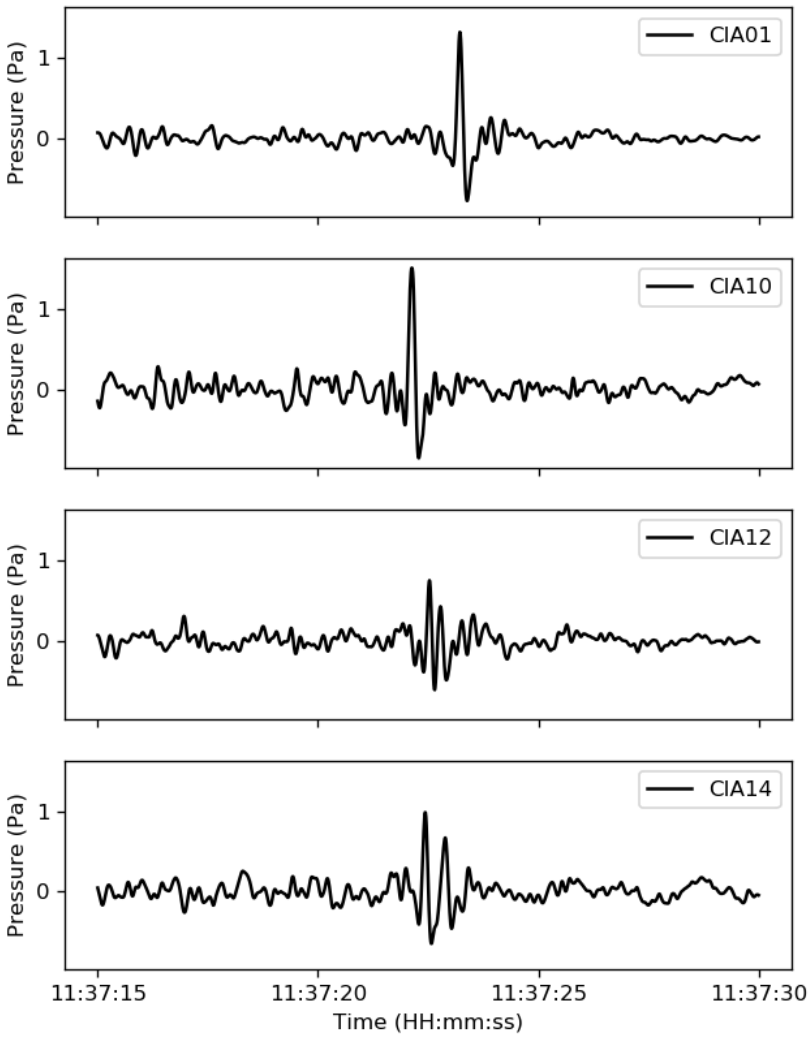

Figure 9: Non time shifted measurements from two ground and two tower sensors

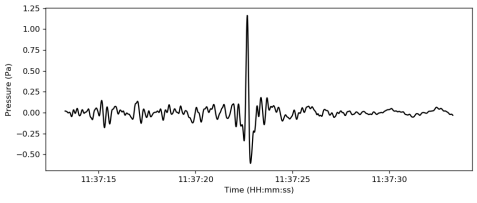

Figure 10: Ground beamform

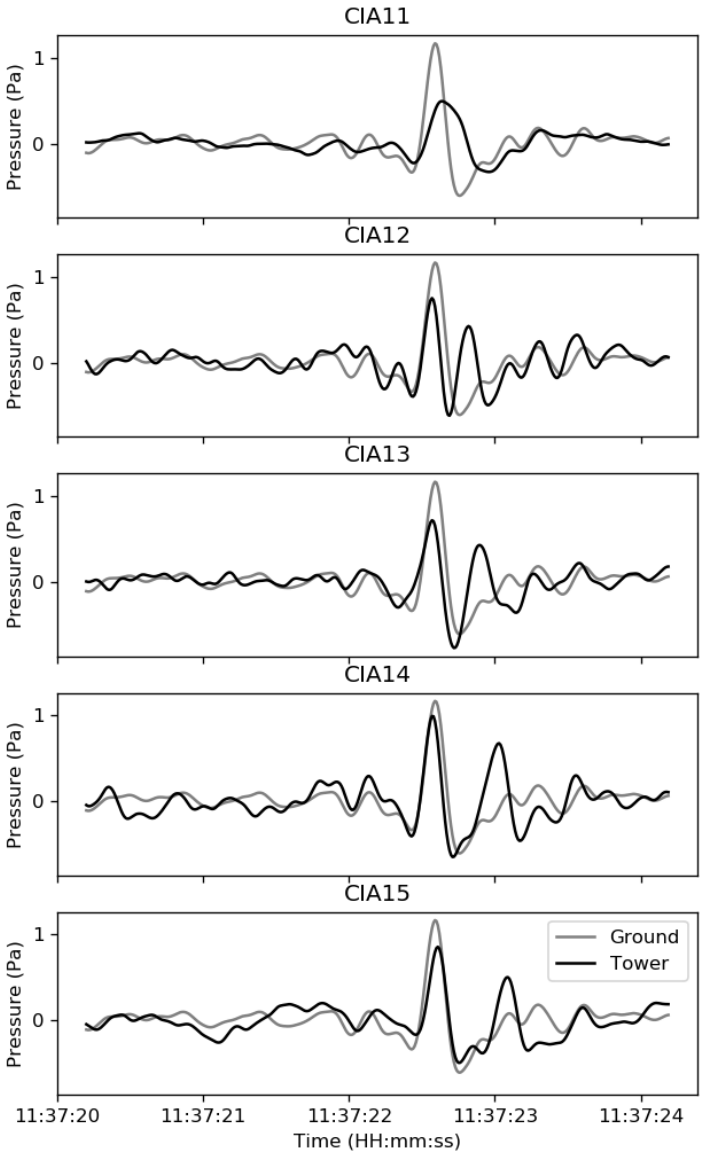

Figure 11: Comparison of tower measurements and ground average before reflection removal

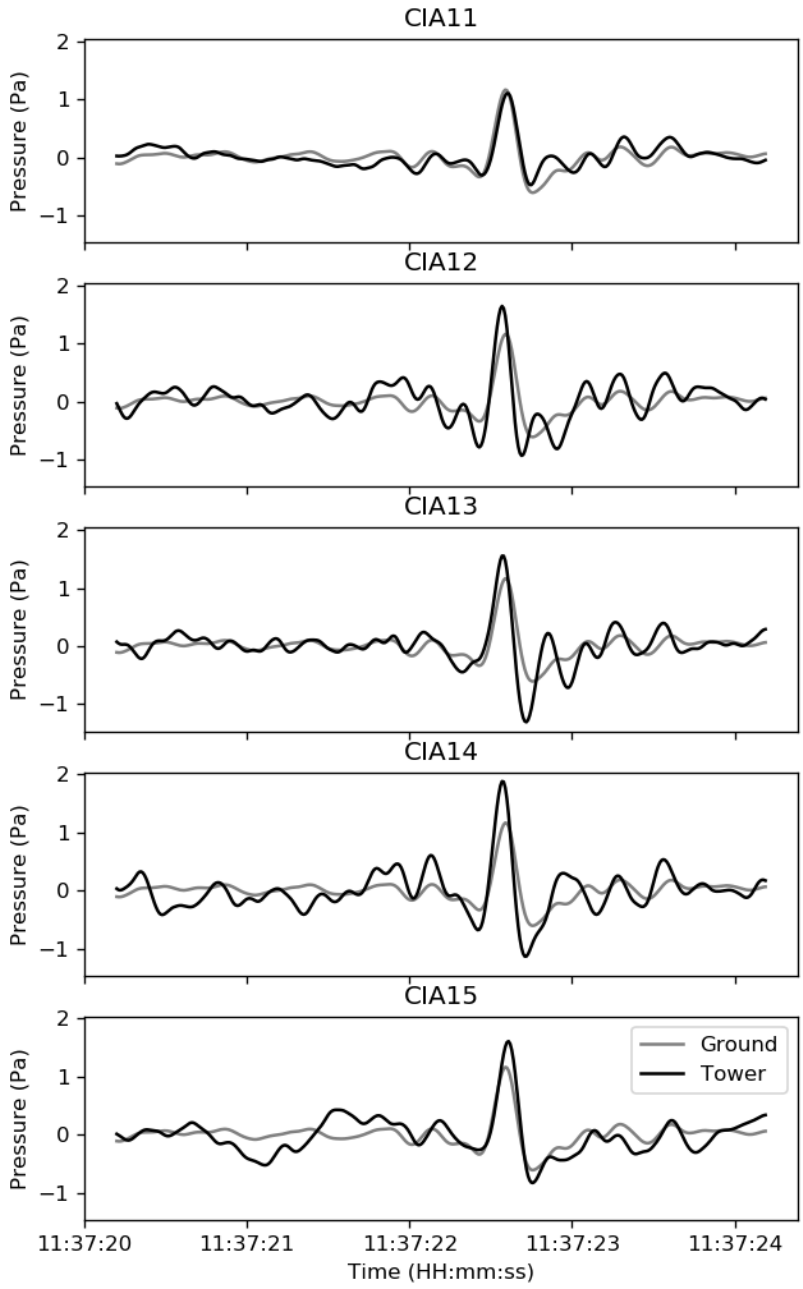

Figure 12: Comparison of cleaned tower measurements and ground average after reflection removal

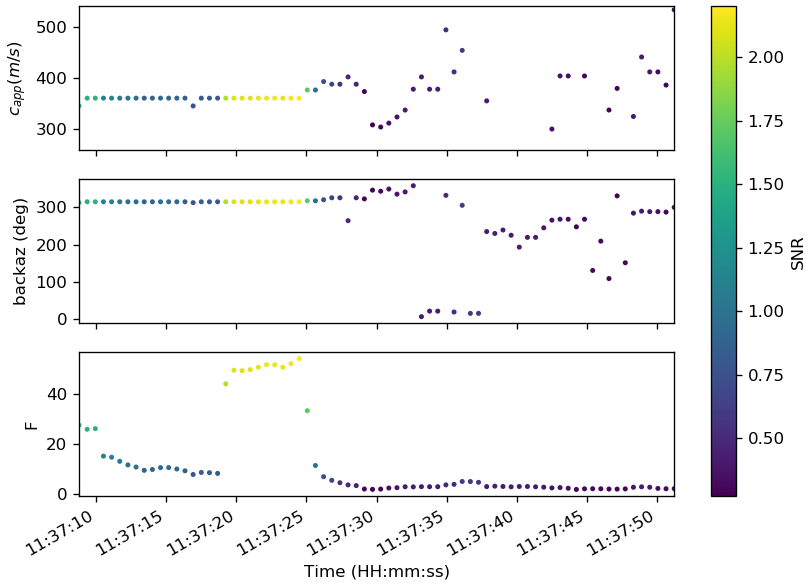

Figure 13: Ground sensors

4 Results

The reflection removal was tested for measurements of a sonic boom above the North Sea on the 24th of January 2017. At the time of the measurements the temperature was $273K$, corresponding to a speed of sound of $331m/s$, calculated using equation 3

Back azimuth degrees are clockwise with respect to the north and inclination is with respect to the horizontal plane. The results from the beamforming process are presented in three groups. In Figure 13 are the results from only the grounds sensors. It shows the apparent velocity, back azimuth and the coherency value (F) over time. The c_{app} and back azimuth for the highest coherency are $360m/s$ and 315° respectively.

Figure 14 shows the results from only the tower sensors. No back azimuth or apparent velocity can be calculated because all sensors have the same x,y coordinates. The figure shows the effective velocity, the speed of sound plus any wind effects, and the inclination with respect to the ground. For the calculation of c_{eff} and the inclination, the x and y components of the slowness from the ground-only results were used. The c_{eff} and the inclination with the highest coherency are $341.86m/s$ and 21.09° respectively.

The results from all the data, ground and the cleaned tower data combined, are shown in Figure 15. For the apparent velocity and back azimuth, the same values as for the ground sensors only are returned. The c_{eff} and the inclination with the highest coherency are $330m/s$ and 23.29° respectively. These values

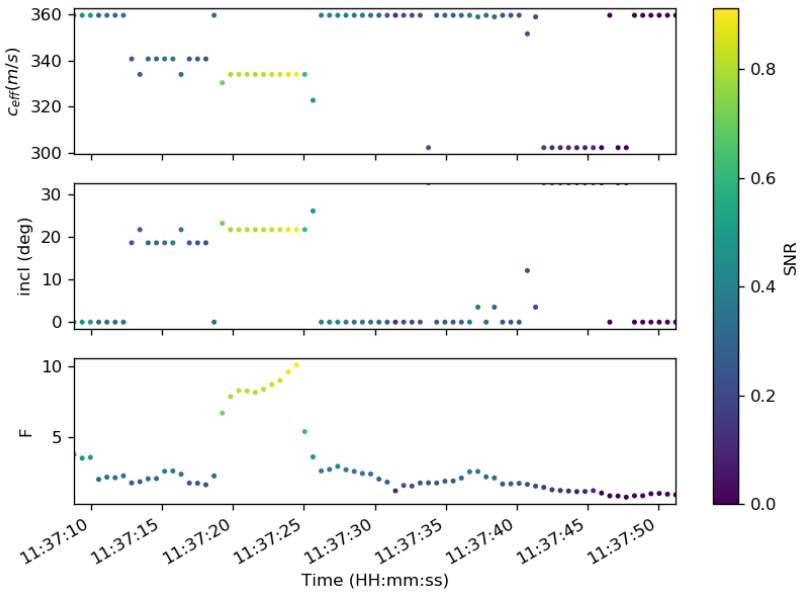

Figure 14: Tower sensors

differ a bit compared to the results from the tower sensors only. This seems to be due to the side effect from the removal of the reflection from the tower measurements. This will receive further evaluation in the next chapter.

Figure 16 shows the direction of the signal plotted on a map. Sonic booms produced by the Dutch Air Force generally occur above the North Sea [Defensie, 2019]. Given the location of the CIA, this would put the source 150km away.

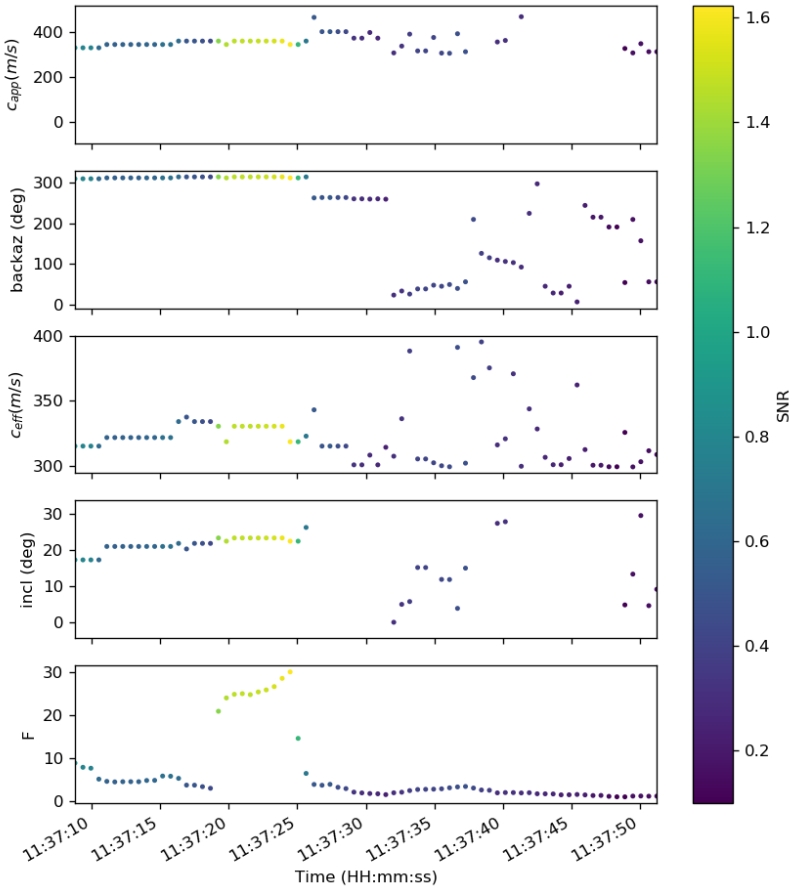

Figure 15: All sensors

Figure 16: The direction of the sonic boom on a map

5 Discussion

The distance of 150km and the inclination correspond to signals that propagate through the stratospheric wave-guide[Evers et al., 2012].

The removal of the reflection from the tower data seems to work fairly well. But there are some limitations. As mentioned in the results section when processing the data from only the tower sensors the results for the inclination differ compared to the results when taking the data from all the sensors. The results from all the sensors is more likely to be correct because this provides a c_{eff} closer to the expected value based on the temperature of $0°C$. And there is an explanation for the difference. This difference seems to be a side effect of the reflection removal process. Both how the reflection gets removed and how the tower measurements get shifted depend on p_z. If no reflection is present at the place of removal an artificial data signal is effectively created. These artificial signals can then increase the coherency values at positions and for shifts where no real signal is present. If no signal is present this tends to result in a p_z of zero. Because the only coherent signal is ground beamform that gets removed from the tower measurements. And even if the ground beamform only contains noise the same noise gets removed from the tower at the same position when p_z is equal to zero.

Figure 17 shows the coherency value as a function of p_z for the tower data only and all events. The black vertical line indicates the maximum value for the tower data and the grey line for all the data. It clearly shows that even though the tower only data returns a lower value for p_z, a closer look shows a more spread out coherency peak. The higher peak is likely a result of the artefacts in the cleaned tower data as a result of non-perfect reflection removal.

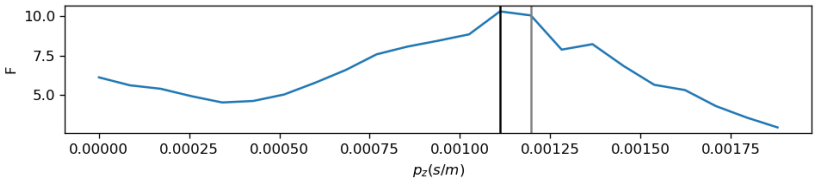

(a) Tower only

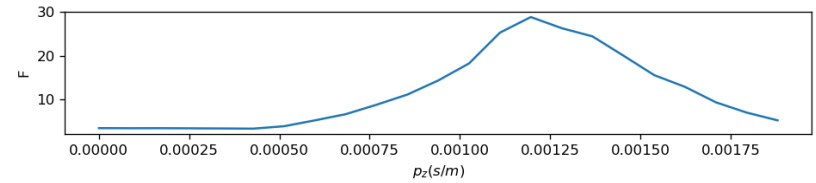

(b) All sensors

Figure 17: Coherency as a function of p_z

Overall the array processing after the reflection removal works as it should. It is quite stable. But the process needs to be tested further on larger data sets. Especially data sets without strong events. As to properly evaluate the effect of potential phantom signals created by the reflection removal process.

References

About Cesar Observatory (n.d.). Accessed on 09.03.2020. URL: http://www.cesar-observatory.nl/index.php?pageID=1003.

Bedard, Alfred and Thomas Georges (2000). 'Atmospheric infrasound'. In: *Acoustics Australia* 28.2, pp. 47–52.

Christie, DR and P Campus (2010). 'The IMS infrasound network: Design and establishment of infrasound stations'. In: *Infrasound monitoring for atmospheric studies*. Springer, pp. 29–75.

Defensie, Ministerie van (2019). *Harde knal door F-16 (sonic boom)*. URL: https://www.defensie.nl/onderwerpen/vliegbewegingen/harde-knal-door-f-16.

Denholm-Price, JCW and JM Rees (1999). 'Detecting waves using an array of sensors'. In: *Monthly weather review* 127.1, pp. 57–69.

Edwards, Wayne N and David N Green (2012). 'Effect of interarray elevation differences on infrasound beamforming'. In: *Geophysical Journal International* 190.1, pp. 335–346.

Evers, LG et al. (2012). 'Anomalous infrasound propagation in a hot stratosphere and the existence of extremely small shadow zones'. In: *Journal of Geophysical Research: Atmospheres* 117.D6.

Fisher, RA (1948). *Statistical Methods of Research Workers: 10th Rev. and Enl. Ed.* Oliver and Boyd.

Gibbons, Steven J, Tormod Kværna and Svein Mykkeltveit (2015). 'Could the IMS infrasound stations support a global network of small aperture seismic arrays?' In: *Seismological Research Letters* 86.4, pp. 1148–1159.

Gossard, Earl E and William H Hooke (1975). 'Waves in the atmosphere: atmospheric infrasound and gravity waves-their generation and propagation'. In: *Atmospheric Science* 2.

Liszka, Ludwik (1974). 'Long-distance propagation of infrasound from artificial sources'. In: *The Journal of the Acoustical Society of America* 56.5, pp. 1383–1388.

Melton, Ben S and Leslie F Bailey (1957). 'Multiple signal correlators'. In: *Geophysics* 22.3, pp. 565–588.

Pierce, Allan D (1990). *Acoustics: An introduction to its physical principles and applications. 1989 Edition.*

Smart, Eugene and Edward A Flinn (1971). 'Fast frequency-wavenumber analysis and Fisher signal detection in real-time infrasonic array data processing'. In: *Geophysical journal international* 26.1-4, pp. 279–284.

Smets, PSM (2018). 'Infrasound and the Dynamical Stratosphere: A new application for operational weather and climate prediction'. Doctoral dissertation. Delft University of Technology.

Smink, Madelon ME et al. (2019). 'A Three-Dimensional Array for the Study of Infrasound Propagation Through the Atmospheric Boundary Layer'. In: *Journal of Geophysical Research: Atmospheres* 124.16, pp. 9299–9313.

Symons, George James et al. (1888). *The eruption of krakatoa: And subsequent phenomena*. Wiley Online Library.